CONFIDENTIAL

Copy
RM L54I10

NACA RM L54I10

NACA

RESEARCH MEMORANDUM

LOW-AMPLITUDE DAMPING-IN-PITCH CHARACTERISTICS OF FOUR TAILLESS SWEPT WING-BODY COMBINATIONS AT MACH NUMBERS FROM 0.85 TO 1.30 AS OBTAINED WITH ROCKET-POWERED MODELS

By Charles T. D'Aiutolo

Langley Aeronautical Laboratory
Langley Field, Va.

NATIONAL ADVISORY COMMITTEE
FOR AERONAUTICS

WASHINGTON

November 24, 1954

CONFIDENTIAL

NATIONAL ADVISORY COMMITTEE FOR AERONAUTICS

RESEARCH MEMORANDUM

LOW-AMPLITUDE DAMPING-IN-PITCH CHARACTERISTICS OF FOUR TAILLESS SWEPT WING-BODY COMBINATIONS AT MACH NUMBERS FROM 0.85 TO 1.30 AS OBTAINED WITH ROCKET-POWERED MODELS

By Charles T. D'Aiutolo

SUMMARY

A free-flight investigation was conducted to determine the damping-in-pitch characteristics of four rocket-powered wing-body combinations between the Mach numbers of 0.85 and 1.30. All models were tested at the same center-of-gravity location (17 percent mean aerodynamic chord) and had identical bodies thereby allowing a direct comparison of the aerodynamic characteristics of the various wings. The wings tested were an aspect-ratio-4, 45° swept composite-plan-form wing (derived from an aspect-ratio-6 wing by increasing the area behind the trailing edge of the inboard 40 percent of the wing), an aspect-ratio-4, 45° swept highly tapered wing, an aspect-ratio-3, 52.5° swept highly tapered wing, and an aspect-ratio-3, 60° swept highly tapered wing. The composite wing had NACA 65A006 airfoil sections parallel to the free stream, whereas the swept highly tapered wings had 65A004 airfoil sections parallel to the free stream.

The results indicated that, although all models were statically stable longitudinally throughout the Mach number range investigated, the dynamic stability of the models was low and differed appreciably for each model. The total damping factor and the slope of the lift curve were about the same order of magnitude resulting in values of the rotational damping-in-pitch derivatives that were either negative (stable) or positive (unstable).

A comparison of the damping was made between a delta wing in combination with a body and a swept wing in combination with a body and the results indicated that at M = 1.16 the delta-wing configuration had better damping characteristics.

INTRODUCTION

Recently a series of systematic experimental investigations has been conducted on tailless aircraft configurations to verify the theoretical predictions of low dynamic longitudinal stability and regions of dynamic instability of these designs (see, for example, refs. 1 to 5). Inasmuch as most of this work was concerned with the delta-wing configurations and very little information is available concerning swept-wing configurations, this investigation was undertaken to determine experimentally the regions of dynamic instability at transonic speeds and low supersonic speeds of some tailless swept-wing airplane configurations.

This report is a continuation of the investigation reported in reference 5 and contains the results from the flight tests, conducted by the Pilotless Aircraft Research Division, of four rocket-powered wing-body combinations. Two of the wings used in these configurations had 45° of sweep and aspect ratios of 4, the only difference being that one was of composite plan form (resulting from a search for an improved design suitable for high-speed flight, see ref. 6) and the other was highly tapered. The third and fourth wings were both of aspect ratio 3 and highly tapered, with one having 52.5° of sweep and the other 60°. The composite wing had NACA 65A006 airfoil sections parallel to the free stream, whereas the swept highly tapered wing had NACA 65A004 airfoil sections parallel to the free stream. The data are presented over a Mach number range of about 0.85 to 1.30 corresponding to a Reynolds number range (based on respective mean aerodynamic chords) of about 7×10^6 to 14×10^6, respectively.

The models were flown at the Langley Pilotless Aircraft Research Station at Wallops Island, Va. The static and dynamic longitudinal stability characteristics of the models were determined by analyzing the oscillations produced in pitch by firing small pulse rocket motors which were mounted to provide thrust normal to the longitudinal axis of the models. The drag characteristics of the models and the stability characteristics were determined from the deceleration portion of the flights.

SYMBOLS

V	velocity of flight, ft/sec
M	Mach number, $\frac{V}{\text{Speed of sound}}$
S	total wing area, sq ft

$\bar{c}$ mean aerodynamic chord, ft

A aspect ratio

A' cross-sectional area of any longitudinal station of complete model, sq ft

l body length, ft

X distance along body measured from nose, ft

ρ air density, slugs/cu ft

R Reynolds number (based on mean aerodynamic chord of respective models)

q free-stream dynamic pressure, lb/sq ft

b total damping factor (logarithmic decrement of pitch oscillations)

P period of short-period oscillations, sec

k reduced-frequency parameter (based on respective mean aerodynamic chords of models), $\frac{\omega \bar{c}}{2V}$

C_L lift coefficient, $C_N \cos \alpha - C_C \sin \alpha$

C_N normal-force coefficient, $\frac{A_N}{g} \frac{W/S}{q}$

$\frac{A_n}{g}$ acceleration normal to reference axis as obtained from accelerometer

C_C chord-force coefficient, $-\frac{A_l}{g} \frac{W/S}{q}$

$\frac{A_l}{g}$ acceleration along reference axis as obtained from accelerometer positive forward

W model weight, lb

C_{L_α} slope of lift curve per degree, $\frac{\partial C_L}{\partial \alpha}$

C_m pitching-moment coefficient, $\frac{\text{Pitching moment}}{qS\bar{c}}$

C_{m_α} static-stability derivative per degree, $\frac{\partial C_m}{\partial \alpha}$

$C_{m_q} = \frac{\partial C_m}{\partial\left(\frac{\dot{\theta}\bar{c}}{2V}\right)}$, per radian

$C_{m_{\dot{\alpha}}} = \frac{\partial C_m}{\partial\left(\frac{\dot{\alpha}\bar{c}}{2V}\right)}$, per radian

C_D drag coefficient, $C_C \cos \alpha + C_N \sin \alpha$

α angle of attack, measured from flight path to fuselage reference line, deg

$\dot{\alpha} = \frac{1}{57.3}\frac{d\alpha}{dt}$, radians/sec

θ angle of pitch, measured from horizontal to fuselage reference line, radians

$\dot{\theta} = \frac{d\theta}{dt}$, radians/sec

t time, sec

ω frequency of short-period oscillation, radians/sec

$\mu = \frac{m}{\rho S \bar{c}}$ relative-density factor

I_Y moment of inertia in pitch, slug-ft^2

m mass, slugs

MODELS AND APPARATUS

Model Description

The general arrangements of the models are shown in figure 1, and a photograph of one of the models is presented in figure 2. Geometric characteristics of the models are presented in table I. Model 1 had an aspect-ratio-4, 45° swept composite plan-form wing (derived from an aspect-ratio-6 wing by increasing the area behind the trailing edge of the inboard 40 percent of the wing) with a taper ratio which varied from about 0.7 for

the outboard panel to about 0.3 for the inboard panel and incorporating NACA 65A006 airfoil sections parallel to the free stream. Model 2 had an aspect-ratio-4, 45° swept highly tapered wing, model 3 had an aspect-ratio-3, 52.5° swept highly tapered wing, and model 4 had an aspect-ratio-3, 60° swept highly tapered wing. The wings of models 2, 3, and 4 incorporated NACA 65A004 airfoil sections parallel to the free stream. Note that the wings of models 1 and 2 were identical in aspect ratio and sweep, but differed in plan-form shape and section thickness, whereas the wings of models 3 and 4 were identical except for wing sweep.

Each model consisted of a basic fuselage to which was attached the wing to be tested. The fuselage was essentially a body of revolution with rather large wing-root fairings for structural purposes and consisted of an ogival nose section which contained the telemeter and a cylindrical body section which contained the wing mount, necessary fairings, the vertical tail, and the sustainer rocket motor. Construction of the fuselage was of aluminum alloy with magnesium skin.

The wings of model 1 were constructed of wood with sheet-steel inlays (for structural purposes), whereas the wings of models 2, 3, and 4 were constructed of solid aluminum. All wings were mounted on the fuselage (as shown in fig. 1) with the resultant center of gravity located at 17 percent of the mean aerodynamic chord during the deceleration portions of the flights.

Each model contained a Cordite sustainer rocket motor and was boosted by a lightweight 5-inch HVAR rocket motor. All models with their boosters were launched from a rail-type launcher (as shown in fig. 3) at an angle of approximately 45°.

The cross-sectional-area distribution of each of the models is presented in figure 4, for possible correlation of drag results.

Instrumentation

Each model contained a standard 4-channel NACA telemeter which transmitted continuous flight measurements of angle of attack (measured by a vane-type instrument located on a sting forward of the nose of the models), normal acceleration of the center of gravity, longitudinal acceleration, and pitot stagnation pressure (measured by a tube located on a strut below the fuselage of the models). (See fig. 1.)

The position of the models in space was determined from an SCR 584 tracking radar and the velocity of the models was obtained by use of the Doppler velocimeter radar. Atmospheric data were obtained from a radiosonde released just prior to each of the model flights. Fixed and tracking motion-picture cameras were used to observe the conditions of the models during the major portion of the flights.

TEST AND ANALYSIS

Test

The data for each model were obtained during the decelerating portion of the flights. The damping-in-pitch data were determined by disturbing each of the models in pitch by a series of four small rocket motors providing thrust normal to the longitudinal axis of the model and located near the rear of the model. These rocket motors were timed to fire in sequence during the decelerating portion of the flights; however, the first small rocket motor to be fired in each of the four models fired prematurely during the latter part of sustainer motor burning. Also, one of the remaining three small rocket motors in model 4 failed to fire, so that damping data from the flight test of model 4 were obtained from the firing of only two of these small rocket motors. Thus, in most instances, reliable damping data could be only obtained from three of the disturbances.

Time histories of angle of attack, lift coefficient, and Mach number covering the decelerating portions of the flight and the times at which the small pulse rockets were fired for each of the four models are shown in figure 5. Also shown are the envelopes drawn for each of the oscillations in pitch that were caused by the firing of the small rocket motors. The static and dynamic longitudinal stability derivatives were obtained from these oscillations.

Data, obtained from spinsonde records, indicated that for each of the four models the rate of roll was approximately zero.

Figures 6, 7, and 8 present, respectively, the variation of air density, velocity, and dynamic pressure with Mach number for each of the tests. These quantities are presented so that a possible correlation of the data obtained from these tests with data obtained from other tests may be made. The range of Reynolds numbers of the tests is plotted against Mach number in figure 9 where the Reynolds number is based on the respective mean aerodynamic chords of the models.

Accuracy

The maximum probable errors in the basic coefficients and angle of attack are as follows:

	M = 0.85	M = 1.25
ΔC_n	0.007	0.003
ΔC_C	0.007	0.003
$\Delta\alpha$, deg	0.20	0.20

These errors are largely due to errors in instrumentation which is a function of the full-scale range of the instruments and errors due to flight conditions. The Mach number as determined from Doppler radar velocity and radiosonde measurements is accurate to better than 2 percent.

Analysis

The analysis of the motions of the models presented in this report are based on the assumption of constant coefficients in the differential equations of motion. (See ref. 7.)

The slope of the lift curve C_{L_α} was found by plotting C_L against α as obtained from the flight records during an oscillation and graphically measuring the slope. The C_{m_α} data that are presented in this paper were calculated by use of the expression

$$C_{m_\alpha} = - \frac{I_Y}{57.3qS\bar{c}}\left(\frac{2\pi}{P}\right)^2 \tag{1}$$

which is based on a single-degree-of-freedom analysis instead of the more usual expression

$$C_{m_\alpha} = - \frac{I_Y}{57.3qS\bar{c}}\left[\left(\frac{2\pi}{P}\right)^2 + b^2\right] \tag{2}$$

which is based on a two-degree-of-freedom analysis. For tailless configurations, the contribution of the total damping factor b to C_{m_α} is negligible when compared to the frequency contribution, so that the single-degree-of-freedom expression given (eq. (1)) allows an accurate determination of C_{m_α}. Values of the total damping factor b were determined by the method presented in the "Analysis" section of reference 5, while values of $C_{m_q} + C_{m_{\dot{\alpha}}}$ were determined by the method presented in appendix A of reference 7.

The maximum value of the reduced-frequency parameter $k = \frac{\omega\bar{c}}{2V}$ (based on respective mean aerodynamic chords) that was determined from these tests was 0.023. Since this value is small, it is believed that the effects of the frequency of the oscillations of the models on the damping in pitch are not important in the determination of the damping-in-pitch derivatives and that the method of reducing the data used in this paper gives good results for these derivatives. Unpublished calculations, comparing the damping in pitch computed for terms to the order of k^3 with the damping in pitch computed for terms to the order of k, indicate that for $k < 0.025$ the difference is about 1 percent. These results

indicated that terms of higher-order frequency are not required in the estimation of the damping-stability derivatives.

RESULTS AND DISCUSSION

The stability parameters of the models presented in this paper were determined from the coasting phase of the flights. Each of the models was tested with the center of gravity located at 17 percent of the mean aerodynamic chord behind the leading edge of the mean aerodynamic chord.

Trim

The trim characteristics of each model are shown in figure 5. Model 3 (A = 3, 52.5° sweep) experienced a small trim change in the transonic speed range; however, it was the largest trim experienced by any of the models tested. At high subsonic speeds, model 3 flew at a trim angle of attack of approximately 1.0° corresponding to a trim lift coefficient of approximately 0.02 and experienced a nose-down trim change at transonic speeds. At supersonic speeds, model 3 flew at a trim angle of attack of approximately 0.5° corresponding to a zero-lift condition.

Lift

The variation of the slope of the lift curve for the four models is presented in figure 10. The test points represent data that were determined from the oscillations produced by the firing of the small pulse rockets and, inasmuch as limited data were obtained, no attempt was made to fair curves through the test data.

Models 1 and 2 (identical aspect ratio and sweep, but different in plan-form shape and section thickness) show about the same variation with Mach number; although, at transonic speeds and supersonic speeds, C_{L_α} of model 2 is somewhat lower than the C_{L_α} of model 1. These differences are not due to wing flexibility since preflight static wing twist indicated that models 1 and 2 had about the same degree of flexibility at transonic and supersonic speeds.

The effect of sweep on C_{L_α} may be seen by comparing model 3 (52.5° sweep) with model 4 (60° sweep) since, except for wing sweepback, the models were the same. Also, both models had about the same degree of wing flexibility. The C_{L_α} data of model 4 are somewhat lower than the C_{L_α} data of model 3 as would be expected since the wing sweep of model 4 was greater than the wing sweep of model 3.

Static Longitudinal Stability

The static longitudinal stability for each of the four models is presented in figure 11 where it is seen that C_{m_α} increases with increasing Mach number through the transonic speed range, then decreases somewhat as the Mach number becomes supersonic. From a comparison of models 1 and 2 (same aspect ratio and sweep, but different in plan-form shape and section thickness), it is seen that at high subsonic and transonic speeds model 1 has greater static longitudinal stability than model 2, while at supersonic speeds the reverse is true. A comparison of model 3 with model 4 (same aspect ratio, but different sweepback) shows that model 3 has slightly greater static longitudinal stability at high subsonic and transonic speeds than model 4, but at supersonic speeds the reverse is true. Note that the static stability of models 2 and 4 increase to a higher Mach number before decreasing than models 1 and 3.

Since all wings were mounted on identical bodies and were tested at the same center-of-gravity location with respect to the mean aerodynamic chord, a comparison of the aerodynamic-center location of the various wings can be made. These values of the aerodynamic-center location appear in the following table:

Mach number	Aerodynamic-center location in percent mean aerodynamic chord for -			
	Model 1	Model 2	Model 3	Model 4
Subsonic	0.361	0.312	0.341	0.332
Transonic . . .	.364	.424	.325	-----
Supersonic . . .	.415	.464	.492	.492

Note that generally for all models as the Mach number increases the aerodynamic-center location moves rearward; however, model 3 indicates a slight forward movement as the Mach number increases from high subsonic speeds to transonic speeds. It is noted that this forward movement of the aerodynamic-center location occurred while model 3 experienced a nose-down trim change (see fig. 5(c)).

Dynamic Longitudinal Stability

Total damping factor.- The total damping factor b was obtained from the time histories of the pitch oscillations (see fig. 5). This total damping factor includes the contribution of moment due to motion along a curved path at constant angle of attack C_{m_q}, the moment due to plunging motion (vertical acceleration) $C_{m_{\dot{\alpha}}}$, and the translational

effect of C_{L_α}. The variation of b with Mach number for each of the four models is presented in figure 12. By use of the method presented in the "Analysis" section of reference 5 it was possible to determine numerous instantaneous values of b at high subsonic speeds for model 1 and at low supersonic speeds for models 2, 3, and 4 such that the solid curves presented in figure 12 represent values that were determined from experimental test data points only. The dashed curves represent fairings between other data points that were obtained for models 1, 2, and 3.

Figure 12 shows that plan-form shape has a pronounced effect on the total damping factor for the low amplitudes reported in this paper. A comparison of models 1 and 2 (identical aspect ratio and sweep, but different in plan-form shape and section thickness) shows that for the composite-plan-form configuration (model 1) the total damping factor b decreases abruptly then increases abruptly for small increments of Mach number at high subsonic speeds, while for model 2 this abrupt decrease followed by an abrupt increase in b over a small range of Mach numbers occurs at low supersonic speeds. These abrupt changes were determined from amplitudes that were less than 0.5° in angle of attack and therefore may not be significant.

The total-damping-factor data for model 3 (52.5° sweep) and model 4 (60° sweep) are also shown in figure 12. Inasmuch as limited data were obtained, it was not possible to determine the effect of sweep on the total damping factor.

Rotational damping-in-pitch derivatives.- The rotational damping-in-pitch derivative for each of the four models was determined by the following expression:

$$C_{m_q} + C_{m_{\dot{\alpha}}} = \frac{2VI_Y}{\bar{c}^2}\left(\frac{2b}{57.3qS} + \frac{C_{L_\alpha}}{mV}\right) \qquad (3)$$

where m is the mass of the model in slugs. It is seen from the foregoing equation (3) that the determination of the value of the rotational damping-in-pitch derivatives is dependent upon differences in the total damping factor b and the translational effect due to C_{L_α}. In the model tests reported in this paper (tailless configurations) the total damping factor and the translational effect of C_{L_α} are about the same order of magnitude resulting in small values of $C_{m_q} + C_{m_{\dot{\alpha}}}$ that are either negative (stable) or positive (unstable). (See figure 13.)

Effect of plan-form shape on the rotational damping-in-pitch derivatives.- A comparison is made in figure 14 between an aspect-ratio-3, tailless delta wing in combination with a body and an aspect-ratio-3, 52.5° swept highly tapered wing in combination with a body (model 3) to

determine the effect of plan-form shape on the rotational damping-in-pitch derivatives. The data for the delta-wing configuration were obtained from reference 5.

From figure 14, it appears that there is little effect of plan-form shape on the rotational damping-in-pitch derivatives at $M = 0.915$ and $M = 1.05$; however, at $M = 1.16$ the delta-wing configuration has better damping characteristics than the swept-wing configuration. Reference 1 also shows that the damping in pitch of the delta-wing plan form is superior to the swept-wing plan form at supersonic speeds.

Drag

The variation of the drag coefficient with Mach number for each of the four models is presented in figure 15. The effect of wing sweep may be seen by comparing models 3 and 4. Model 4 has lower drag throughout the Mach number range than model 3 as would be expected since model 4 has a greater wing sweep than model 3. An indication of the effect of plan form may be made by comparing models 1 and 2 where it is seen that the composite plan form has considerably better drag characteristics than the conventional swept plan form even though the wing of the composite plan form was somewhat thicker than that of the conventional swept plan form.

CONCLUSIONS

From the results of the free-flight tests of four wing-body combinations incorporating identical bodies and tested at the same center-of-gravity location of 17 percent mean aerodynamic chord and consisting of an aspect-ratio-4, 45° swept composite wing, an aspect-ratio-4, 45° swept highly tapered wing, an aspect-ratio-3, 52.5° swept highly tapered wing, and an aspect-ratio-3, 60° swept highly tapered wing, the following conclusions may be stated:

1. All models were statically stable throughout the Mach number range investigated ($M = 0.85$ to 1.30).

2. For the low amplitudes reported in this paper, the total damping factor was affected by plan-form shape, whereas the rotational damping-in-pitch derivatives of the models were low throughout the Mach number range investigated and differed appreciably between models. Inasmuch as the damping-in-pitch derivatives were low, the total damping factor consisted mainly of the contribution of the slope of the lift curve.

3. At $M = 1.16$ and for the wings with aspect ratio 3, the delta-wing configuration had better rotational damping-in-pitch characteristics than the swept-wing configuration.

Langley Aeronautical Laboratory,
National Advisory Committee for Aeronautics,
Langley Field, Va., August 27, 1954.

REFERENCES

1. Tobak, Murray: Damping in Pitch of Low-Aspect-Ratio Wings at Subsonic and Supersonic Speeds. NACA RM A52L04a, 1953.

2. Beam, Benjamin H.: The Effects of Oscillation Amplitude and Frequency on the Experimental Damping in Pitch of a Triangular Wing Having an Aspect Ratio of 4. NACA RM A52G07, 1952.

3. Henderson, Arthur, Jr.: Investigation at Mach Numbers of 1.62, 1.93, and 2.41 of the Effect of Oscillation Amplitude on the Damping in Pitch of Delta-Wing—Body Combinations. NACA RM L53H25, 1953.

4. Kemp, William B., and Becht, Robert E.: Damping-in-Pitch Characteristics at High Subsonic And Transonic Speeds of Four 35° Sweptback Wings. NACA RM L53G29a, 1953.

5. D'Aiutolo, Charles T.: Low-Amplitude Damping-in-Pitch Characteristics of Tailless Delta-Wing—Body Combinations at Mach Numbers From 0.80 to 1.35 As Obtained With Rocket-Powered Models. NACA RM L54D29, 1954.

6. Wolhart, Walter D.: Static Longitudinal Stability Characteristics of a Composite-Plan-Form Wing Model Including Some Comparisons With a 45° Sweptback Wing at Transonic Speeds. NACA RM L54F24, 1954.

7. Gillis, Clarence L., Peck, Robert F., and Vitale, A. James: Preliminary Results From a Free-Flight Investigation at Transonic and Supersonic Speeds of the Longitudinal Stability and Control Characteristics of an Airplane Configuration With a Thin Straight Wing of Aspect Ratio 3. NACA RM L9K25a, 1950.

TABLE I.- GEOMETRIC CHARACTERISTICS OF THE MODELS

	Model 1	Model 2	Model 3	Model 4
Wing:				
Total area, sq ft	5.76	4.40	4.40	4.40
Span, ft	4.82	4.20	3.64	3.64
Aspect ratio	4	4	3	3
Mean aerodynamic chord, ft	1.59	1.21	1.39	1.39
Sweepback of quarter-chord, deg	45	45	52.5	60
Dihedral, deg	0	0	0	0
Taper ratio	[a]0.715, [b]0.288	0.20	0.20	0.20
NACA airfoil sections parallel to free stream	65A006	65A004	65A004	65A004
Fuselage:				
Length, in.	75.00	75.00	75.00	75.00
Fineness ratio	10.70	10.70	10.70	10.70
Miscellaneous:				
Model weight, lb	128.25	121.00	125.00	123.50
Moment of inertia in pitch, I_y, slug-ft^2	10.96	10.30	10.10	10.50
Center-of-gravity position, percent M.A.C.	17	17	17	17
Wing loading, lb/sq ft	22.2	27.5	28.4	28.0
Relative density factor, μ -				
At M = 0.85	222	356	346	342
At M = 1.25	199	320	298	295

[a]Outboard.

[b]Inboard.

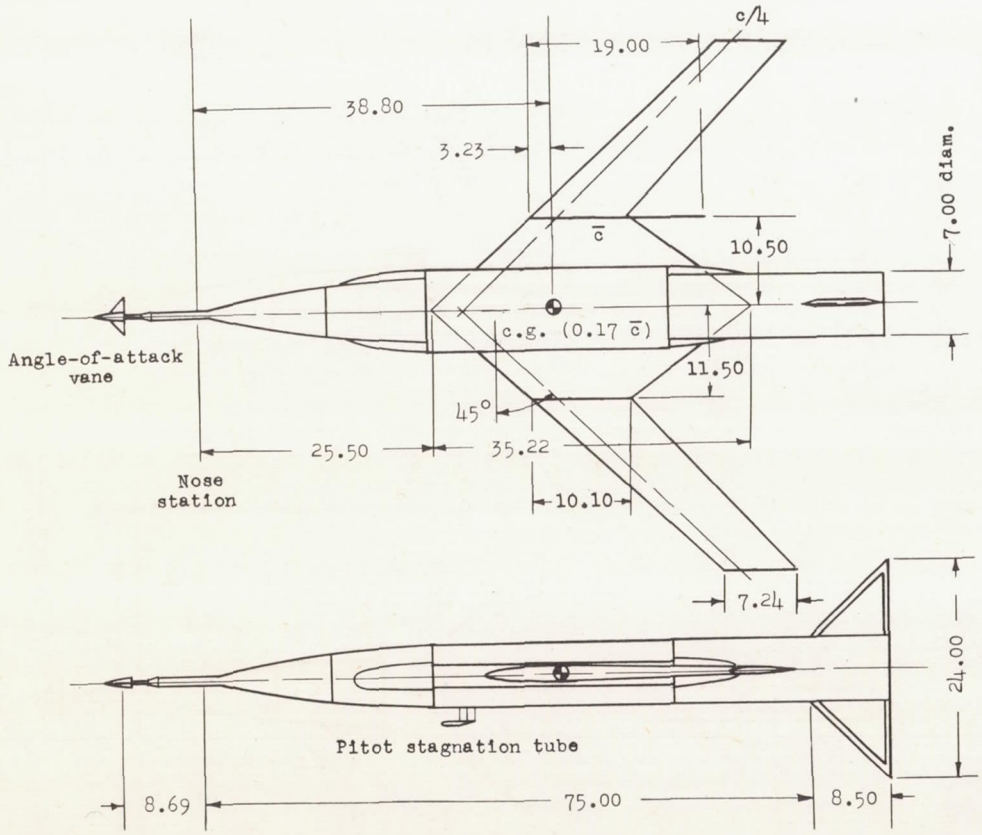

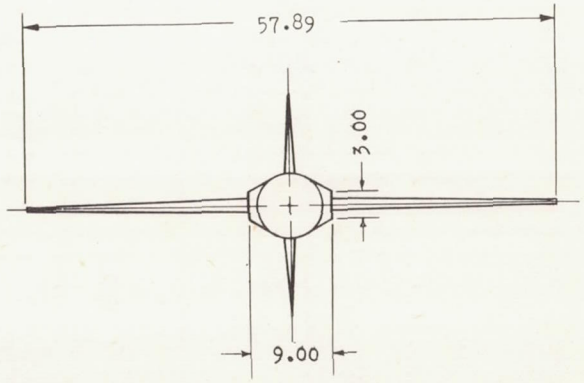

(a) Model 1. A = 4; airfoil sections, NACA 65A006.

Figure 1.- General arrangement of models. All dimensions in inches unless otherwise noted.

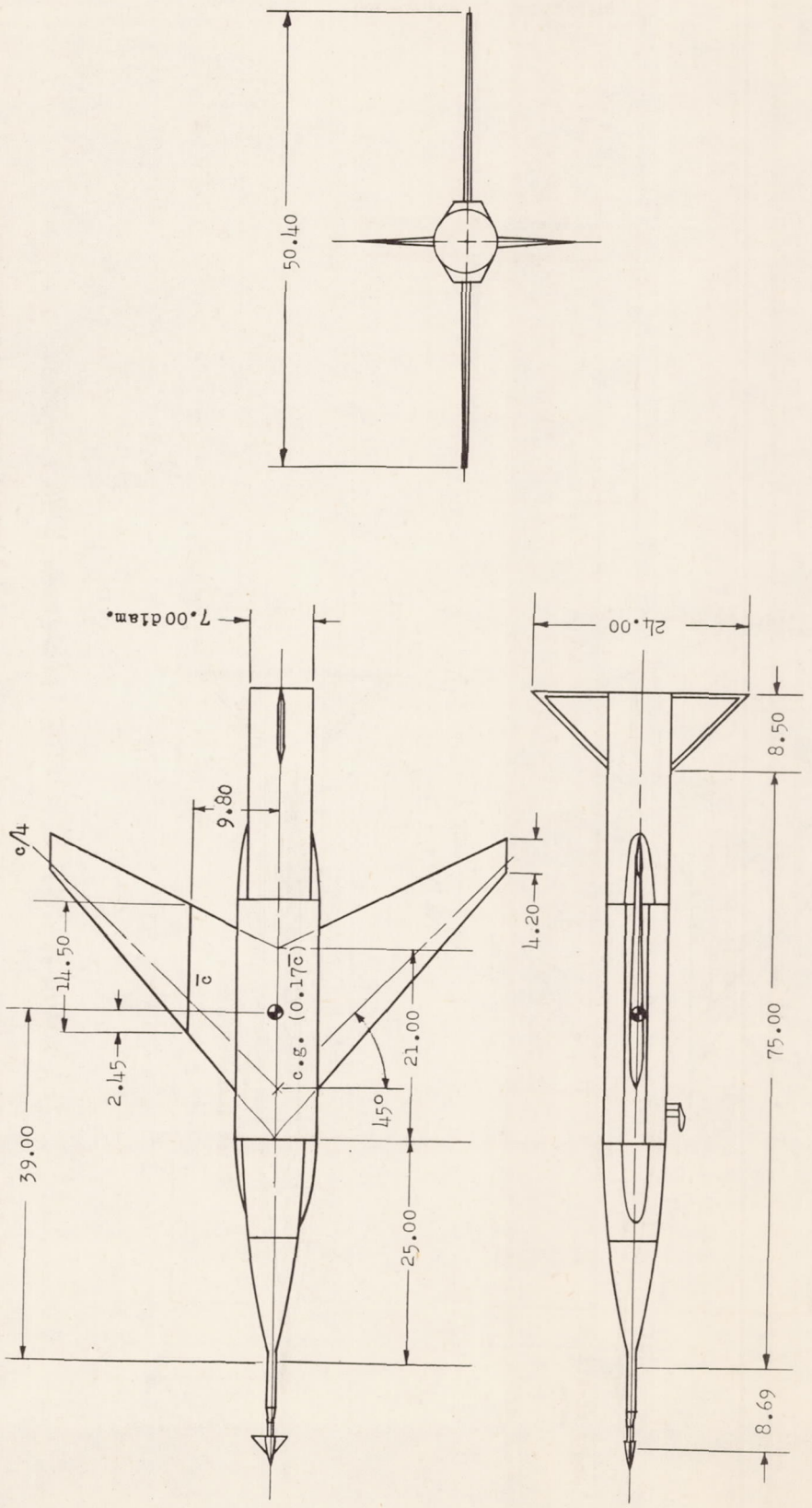

(b) Model 2. A = 4; airfoil sections, NACA 65A004.

Figure 1.- Continued.

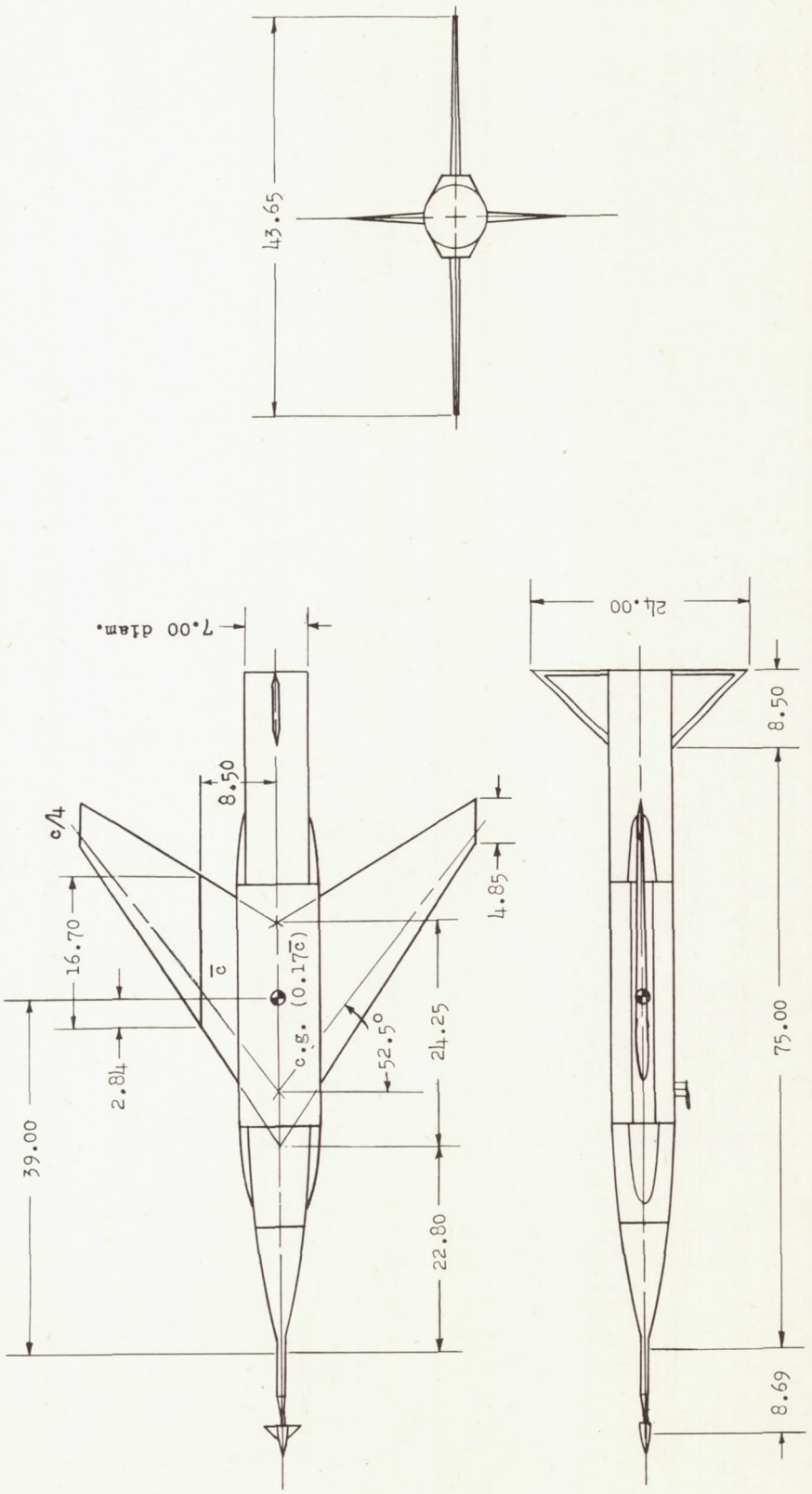

(c) Model 3. A = 3; airfoil sections, NACA 65A004.

Figure 1.- Continued.

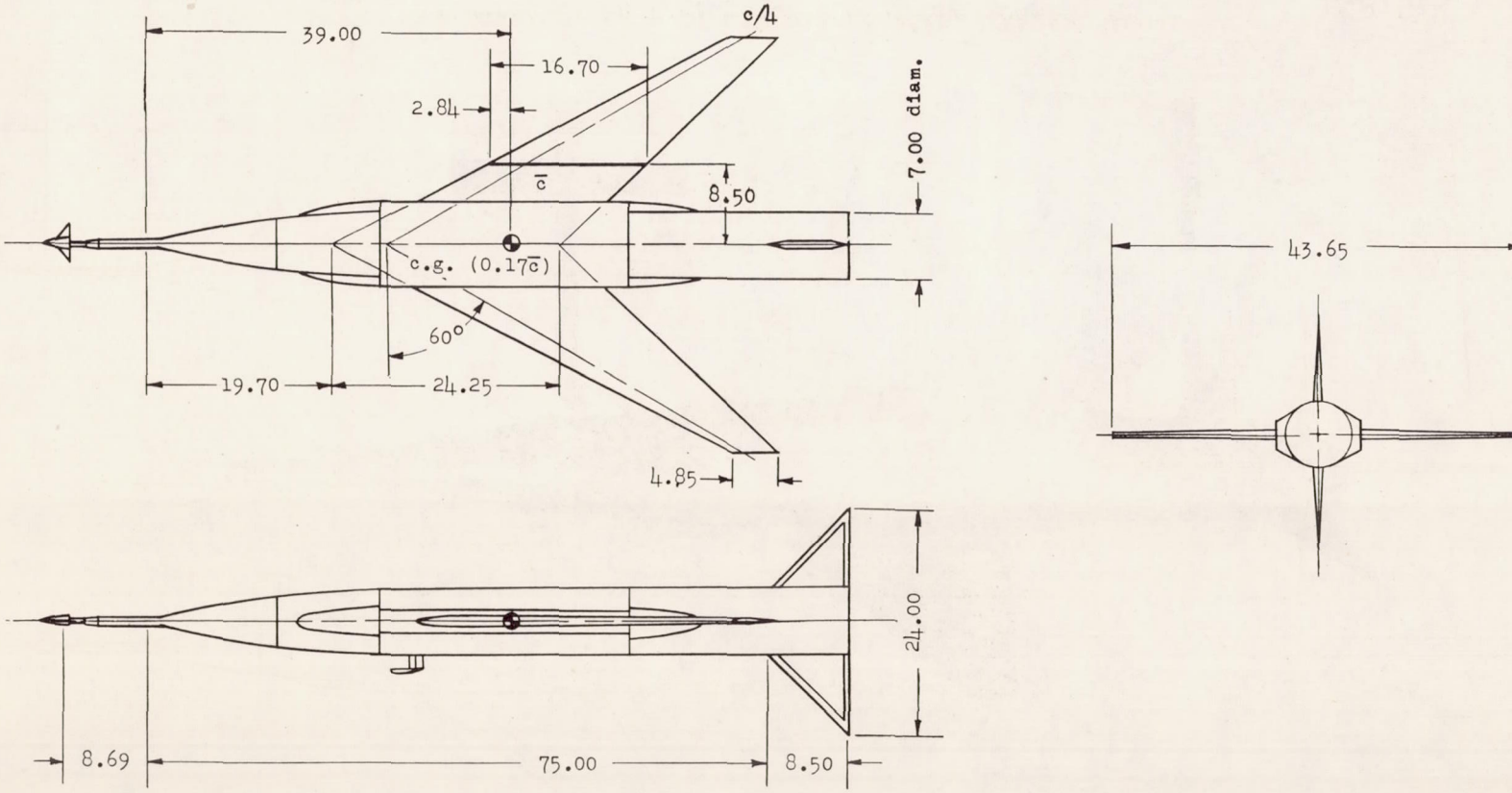

(d) Model 4. A = 3; Airfoil sections, NACA 65A004.

Figure 1.- Concluded.

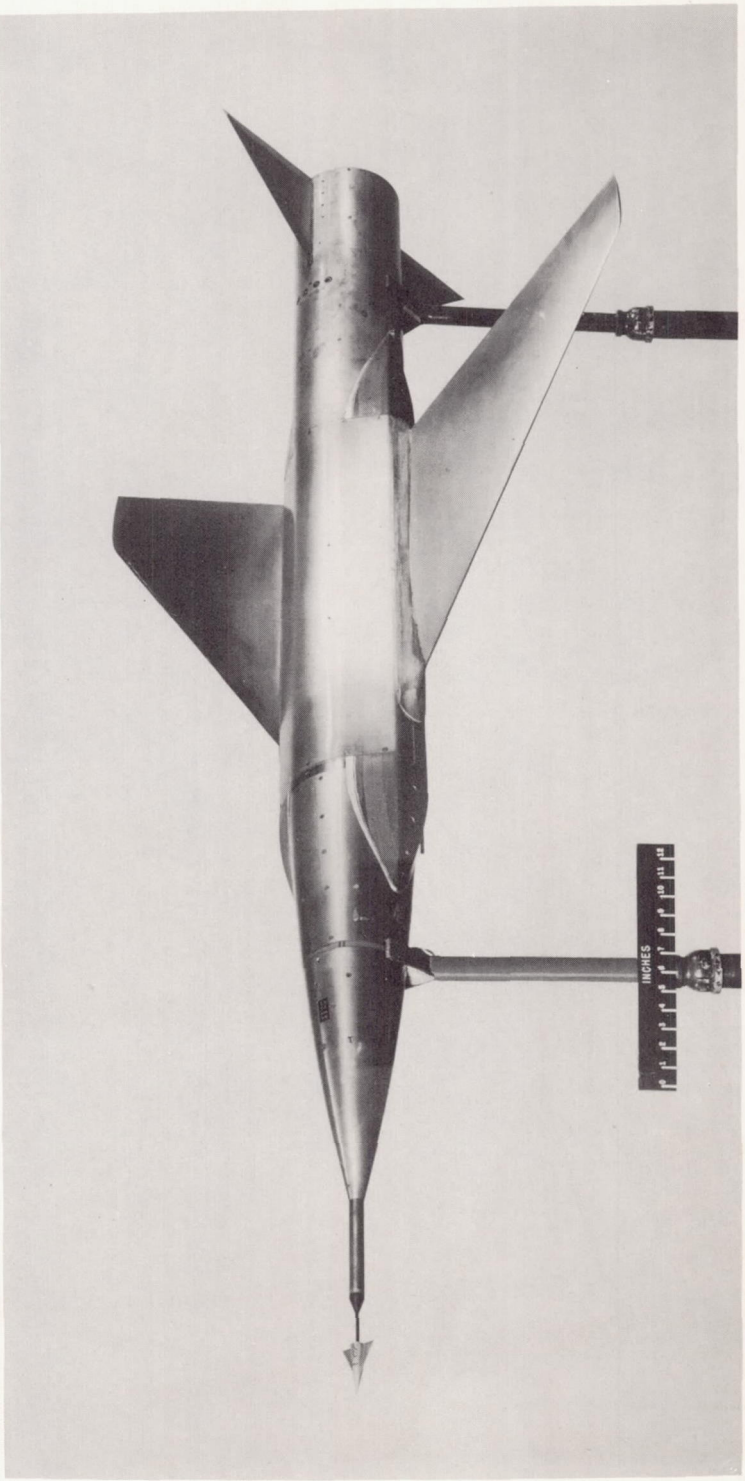

L-81813.1

Figure 2.- Photograph of one of the models.

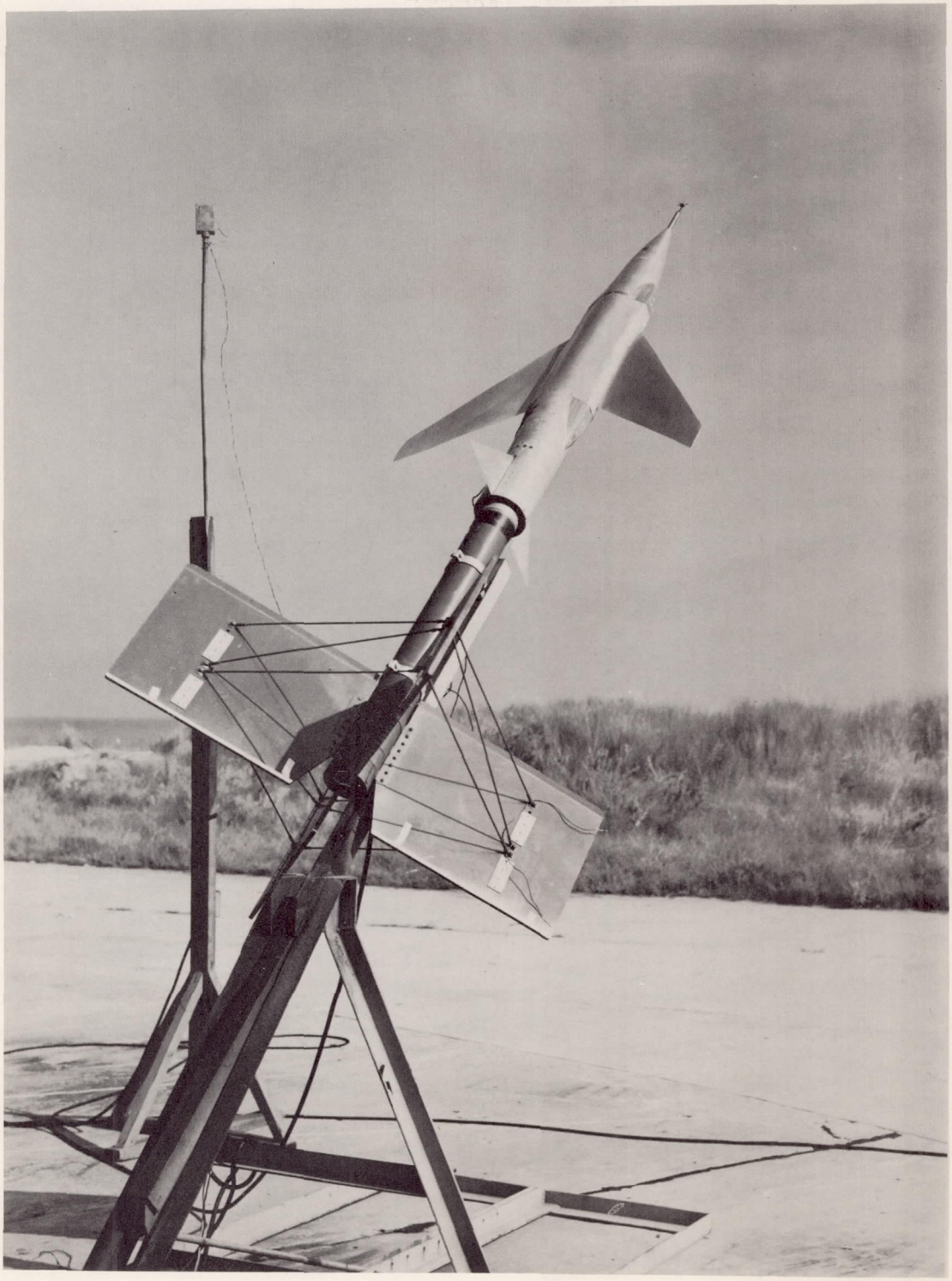

Figure 3.- Photograph of one of the models on the launcher. L-81915.1

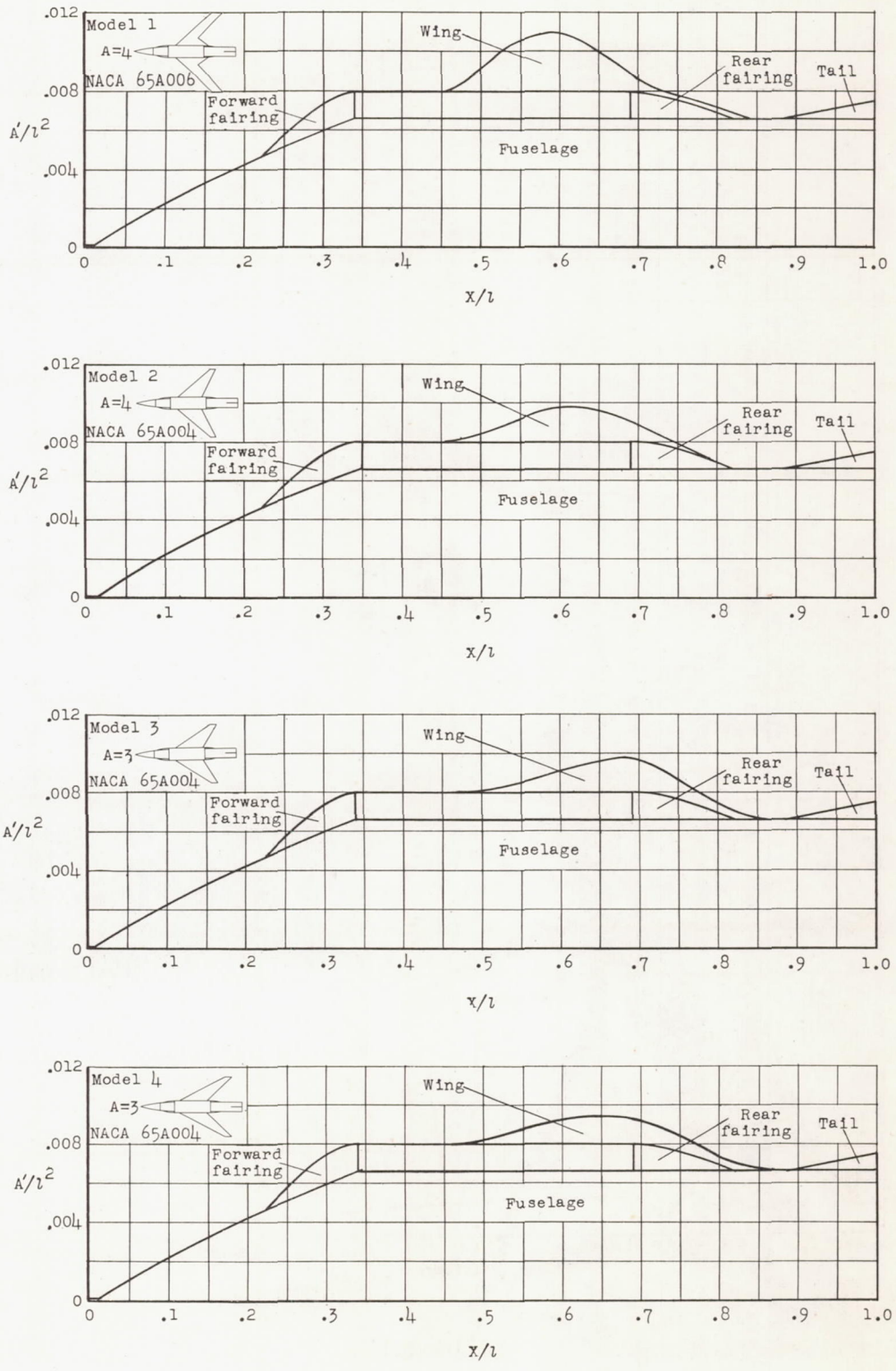

Figure 4.- Longitudinal distribution of cross-sectional area.

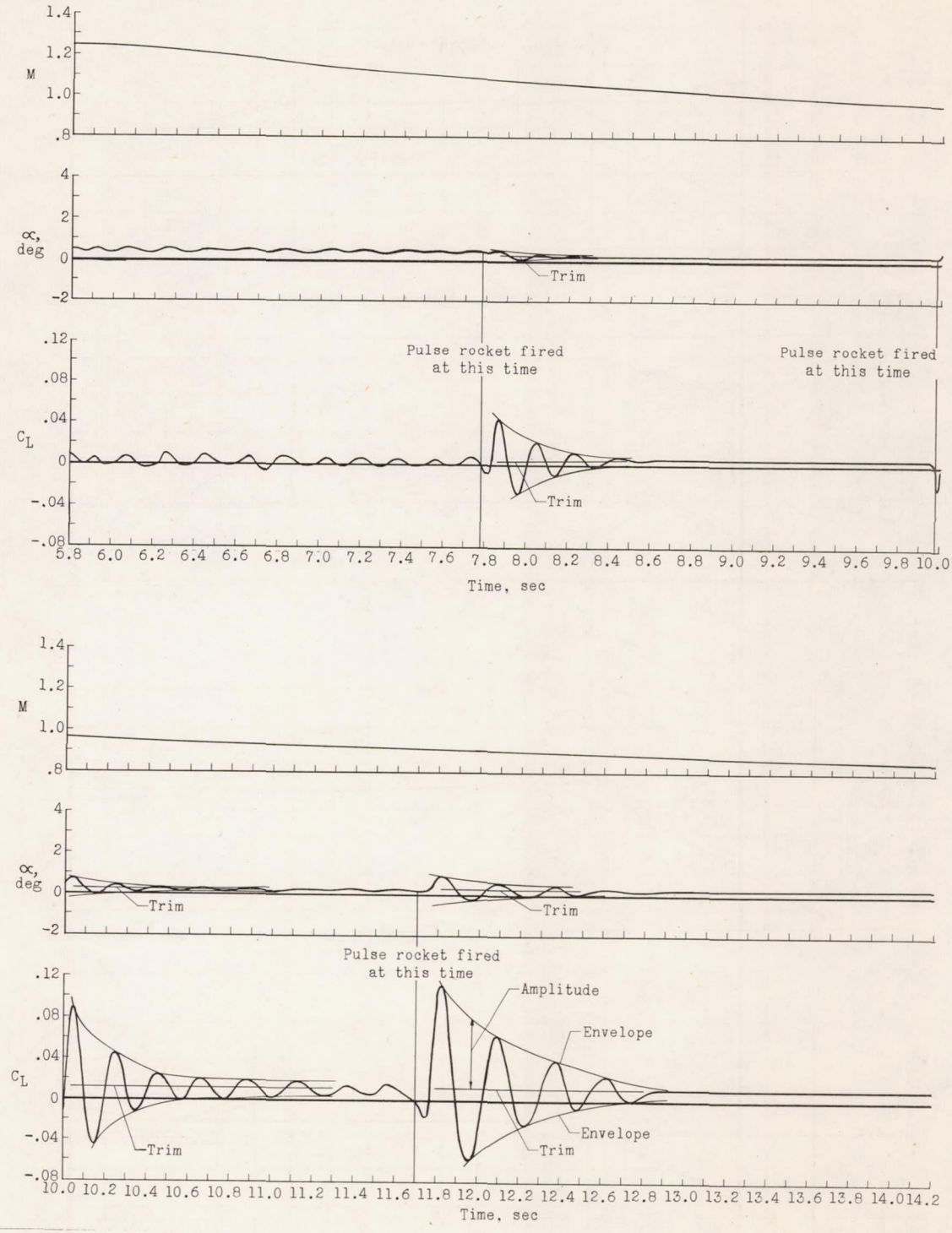

(a) Model 1.

Figure 5.- Time history of flights showing envelopes of the oscillations, trim values, and the times where the pulse rockets were fired.

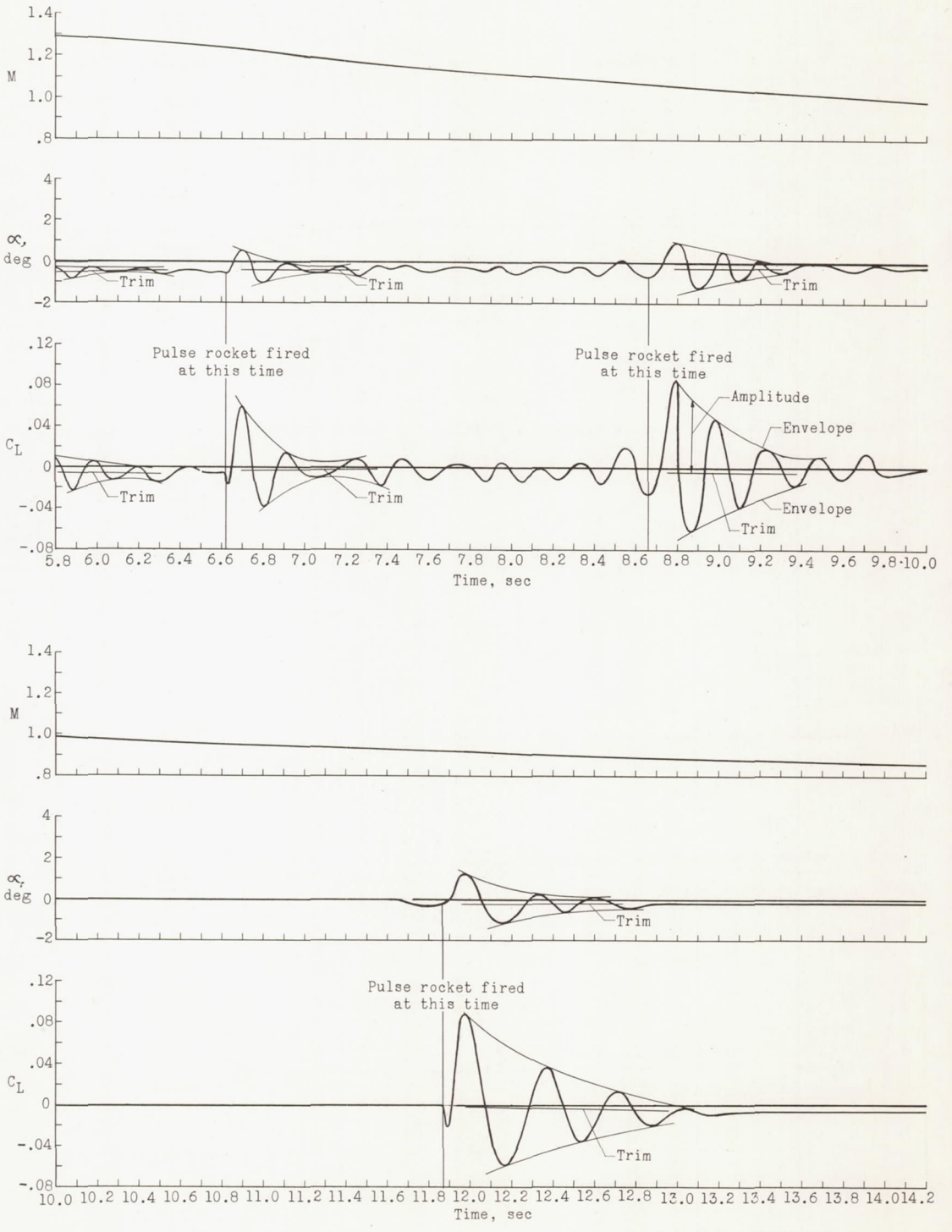

(b) Model 2.

Figure 5.- Continued.

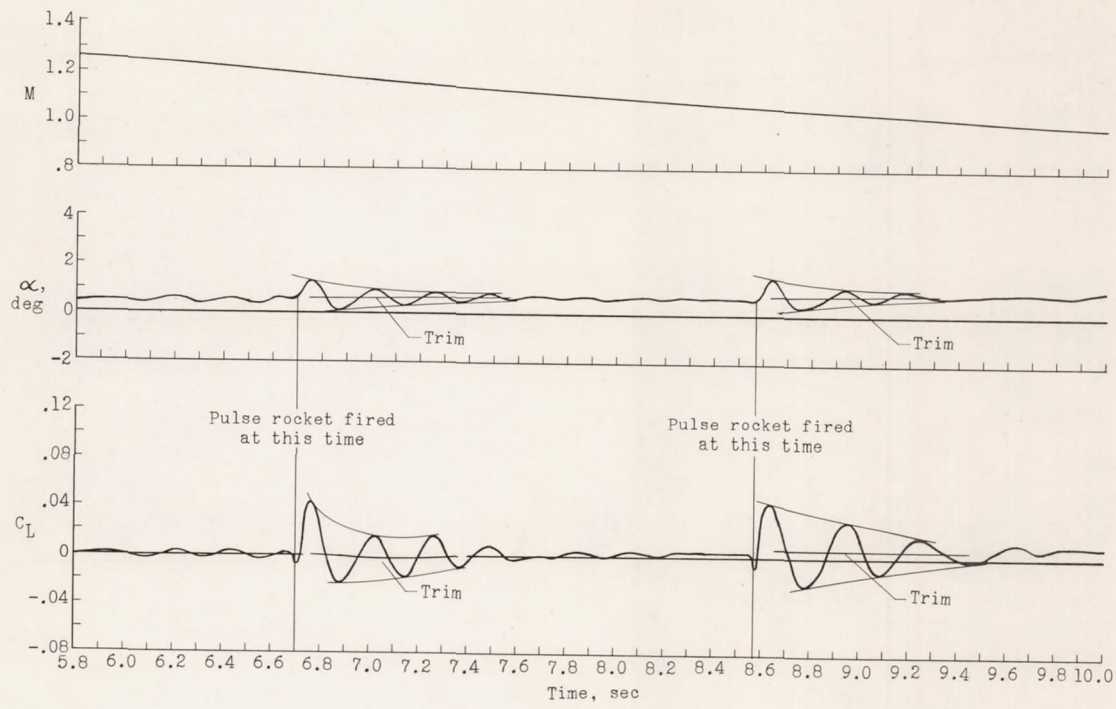

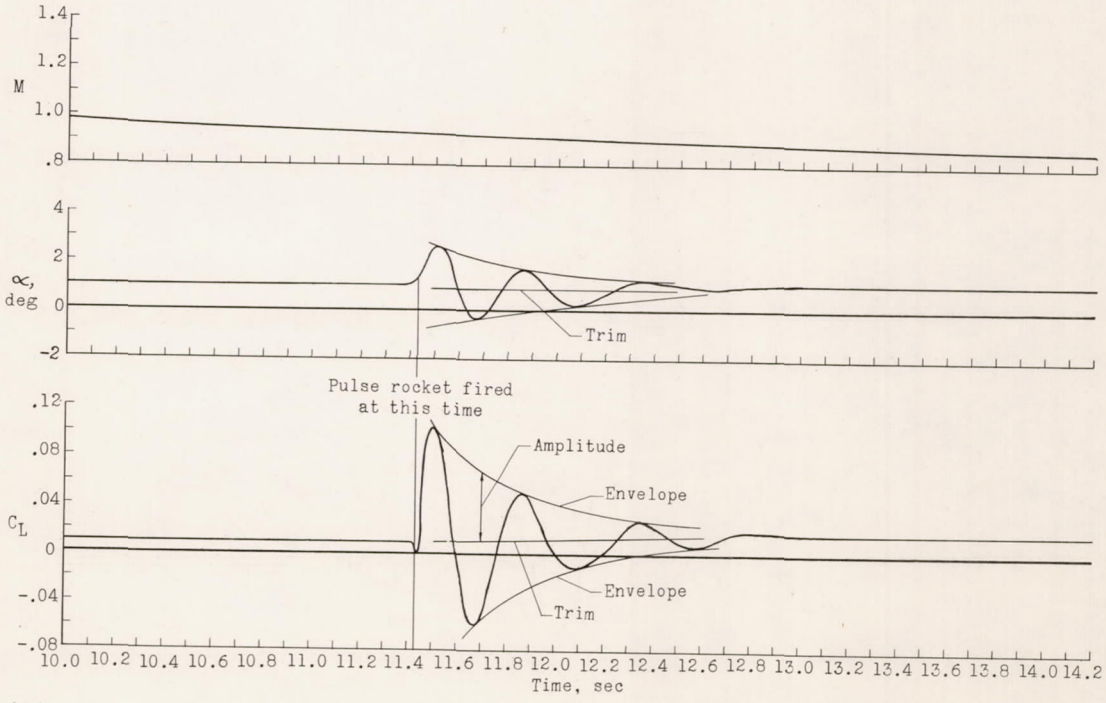

(c) Model 3.

Figure 5.- Continued.

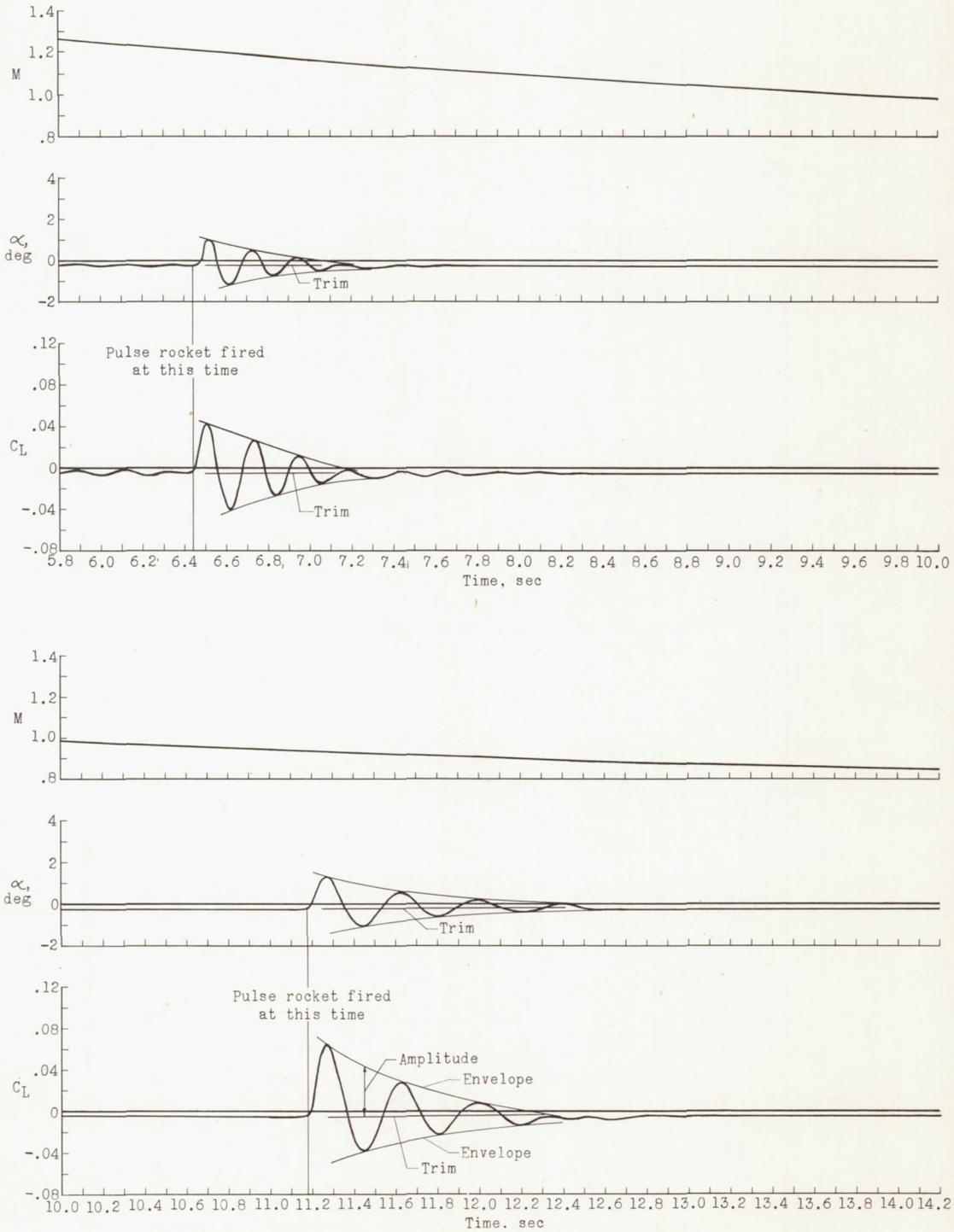

(d) Model 4.

Figure 5.- Concluded.

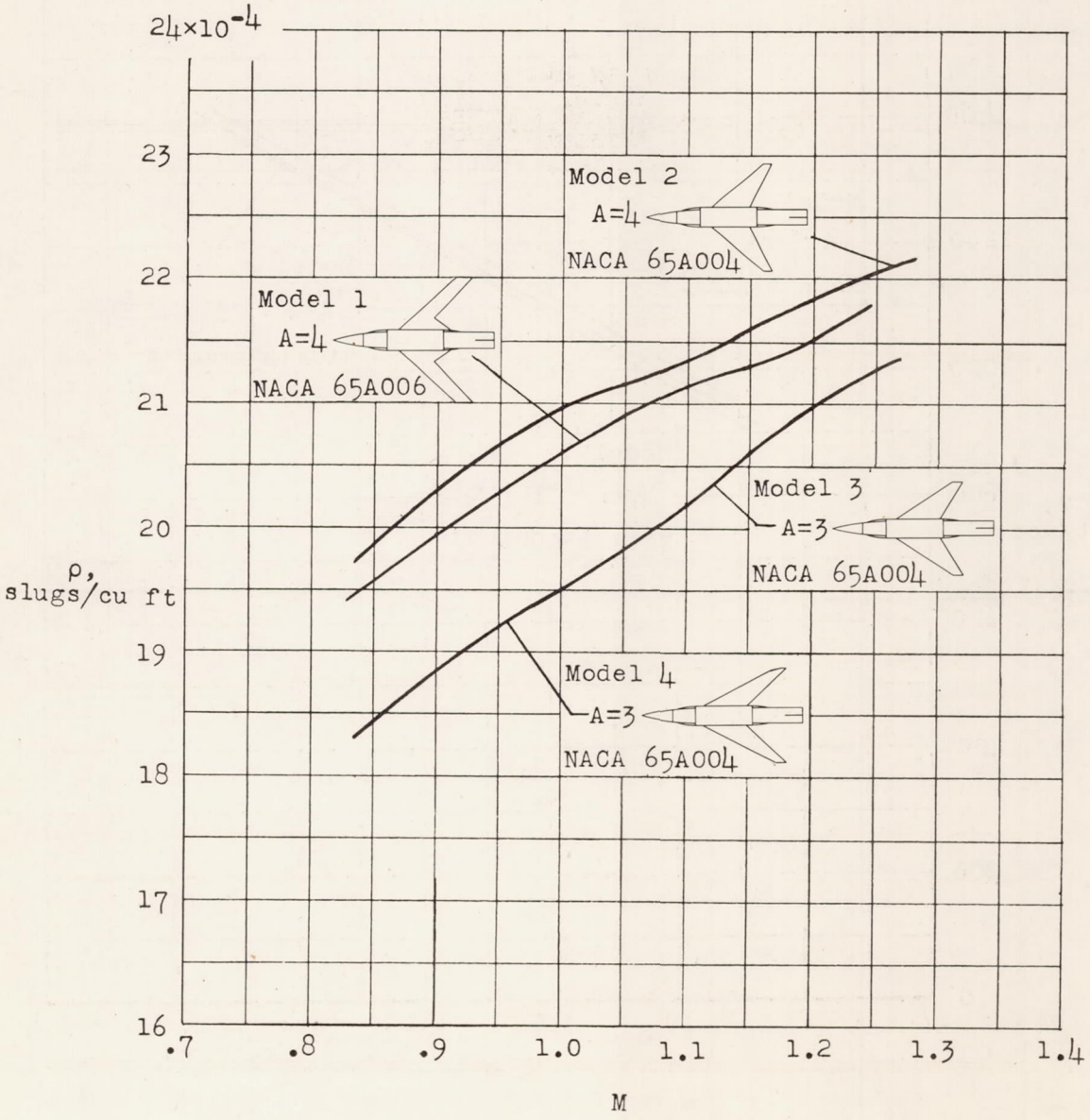

Figure 6.- Variation of air density with Mach number.

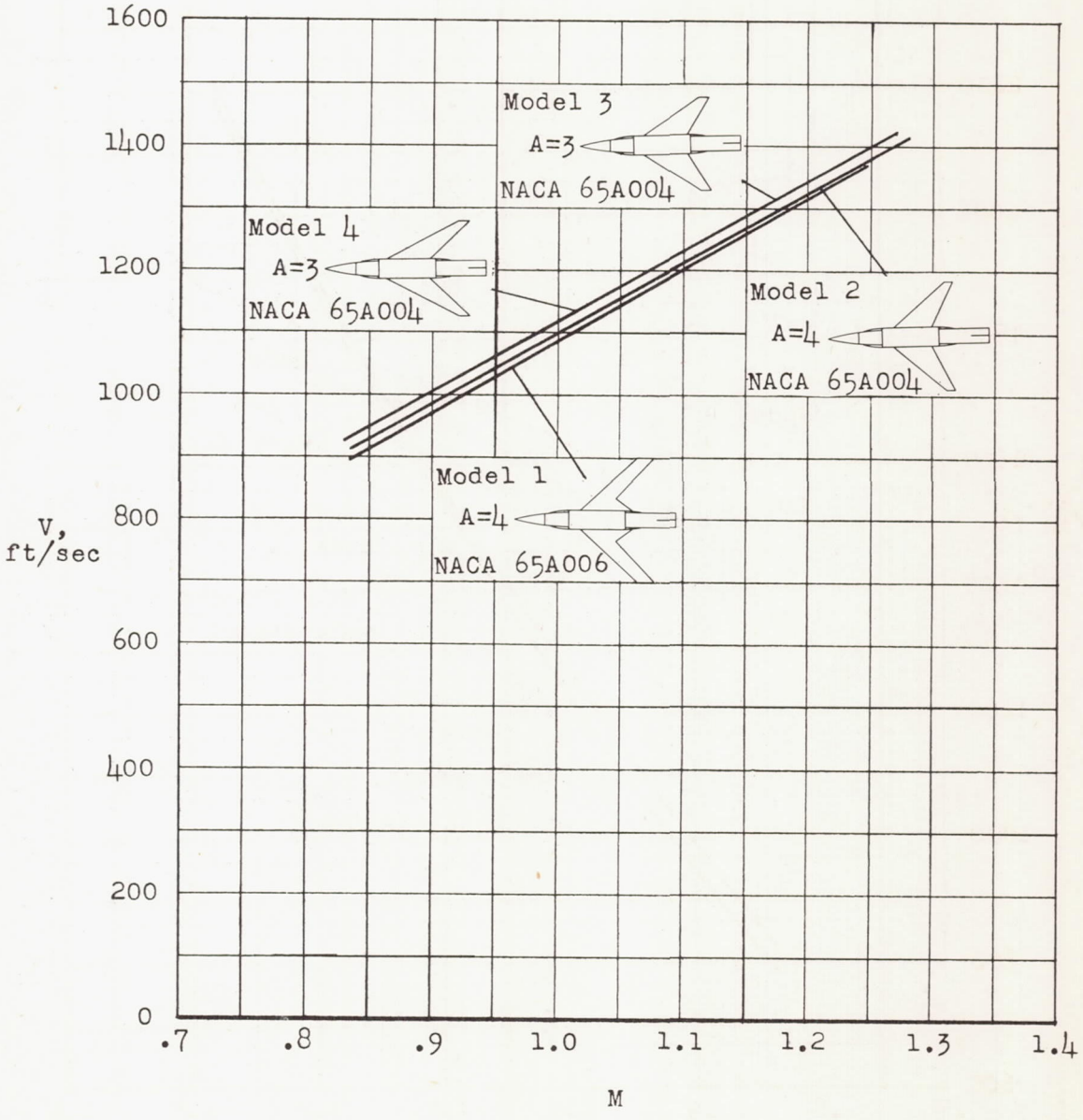

Figure 7.- Variation of velocity with Mach number.

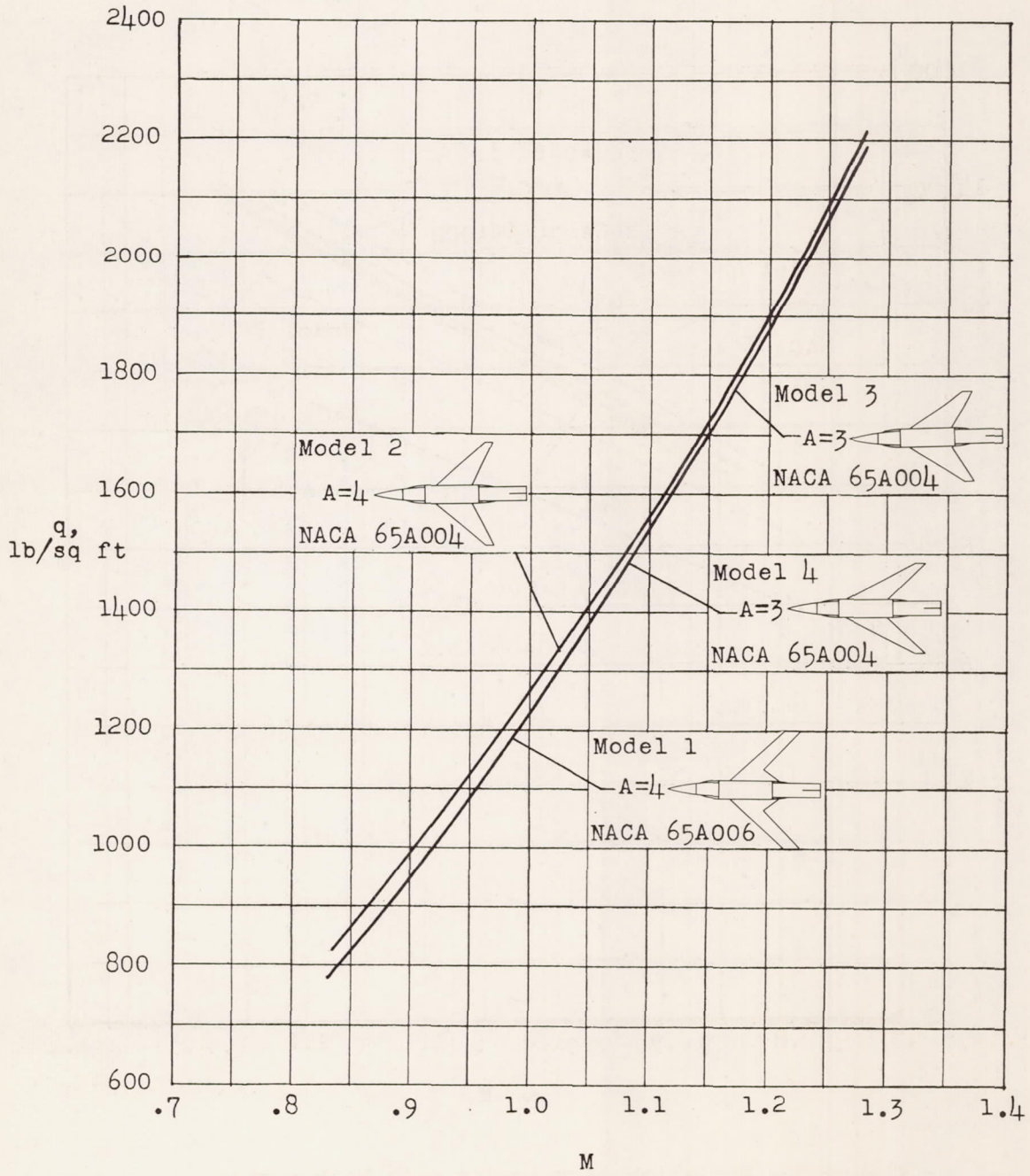

Figure 8.- Variation of dynamic pressure with Mach number.

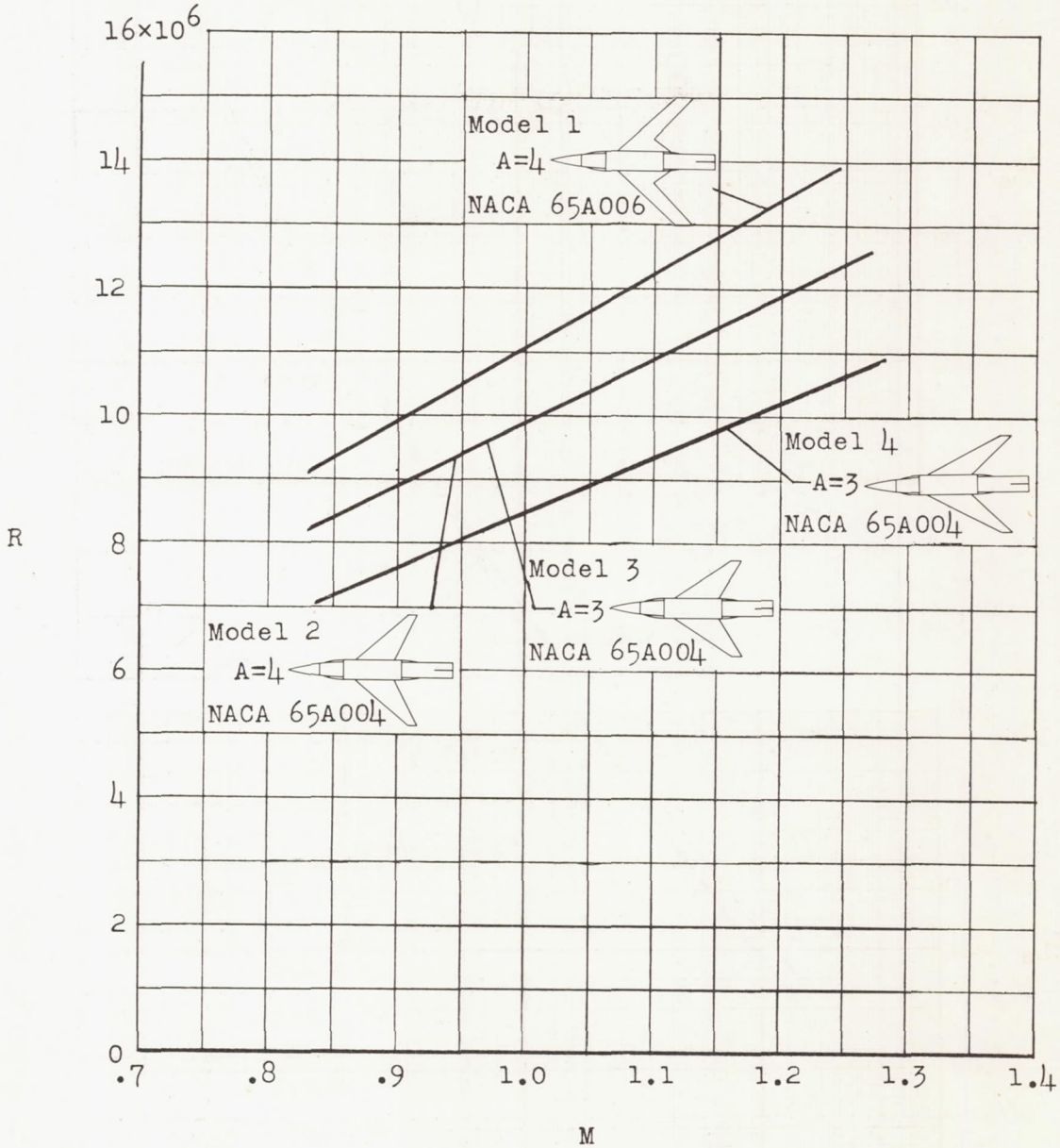

Figure 9.- Variation of Reynolds number, based on respective mean aerodynamic chord, with Mach number.

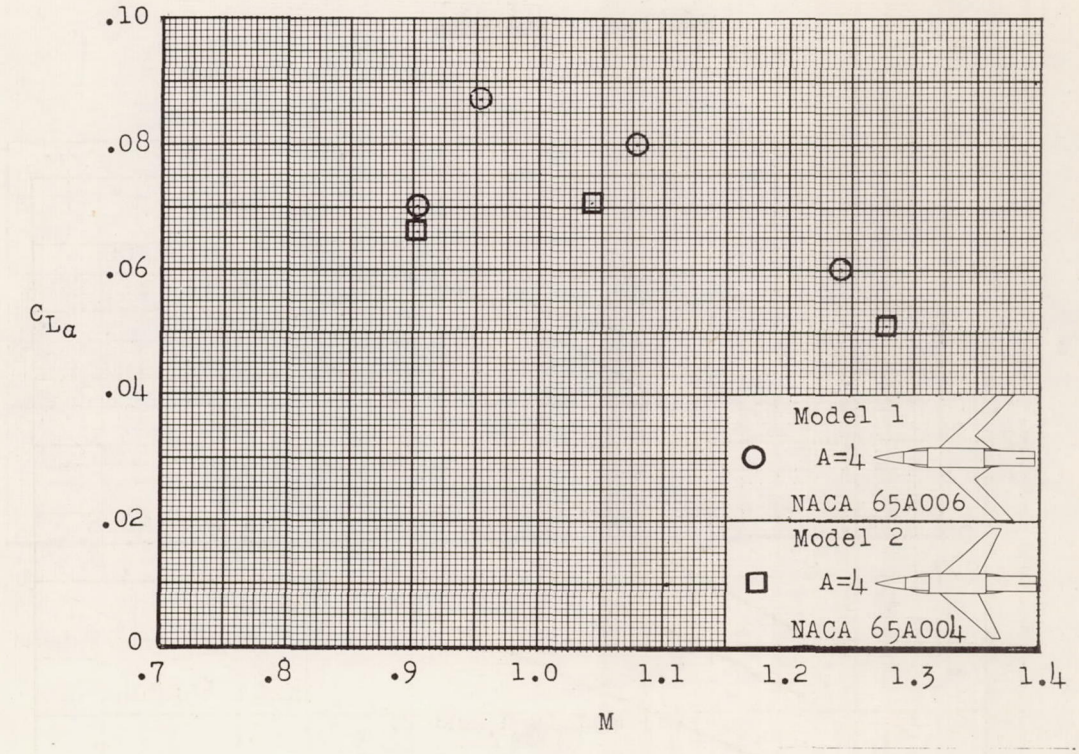

(a) Models 1 and 2.

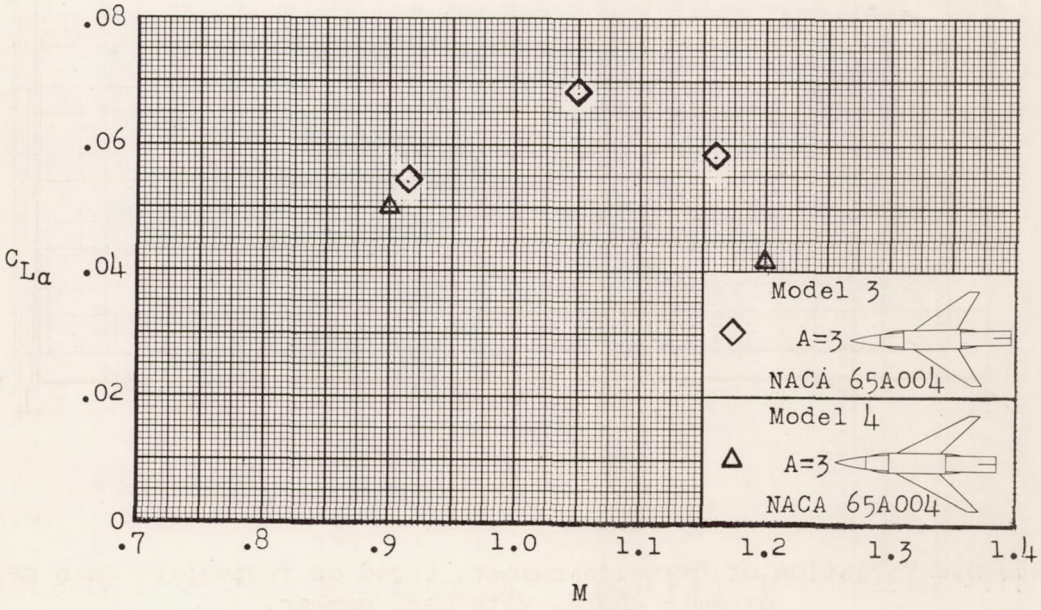

(b) Models 3 and 4.

Figure 10.- Variation of the slope of the lift curve with Mach number.

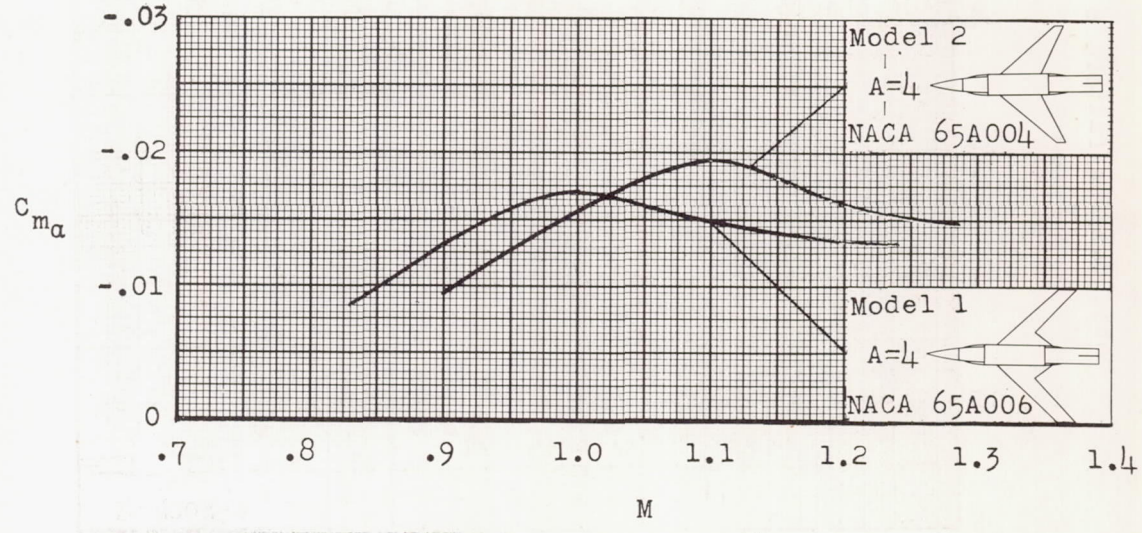

(a) Models 1 and 2.

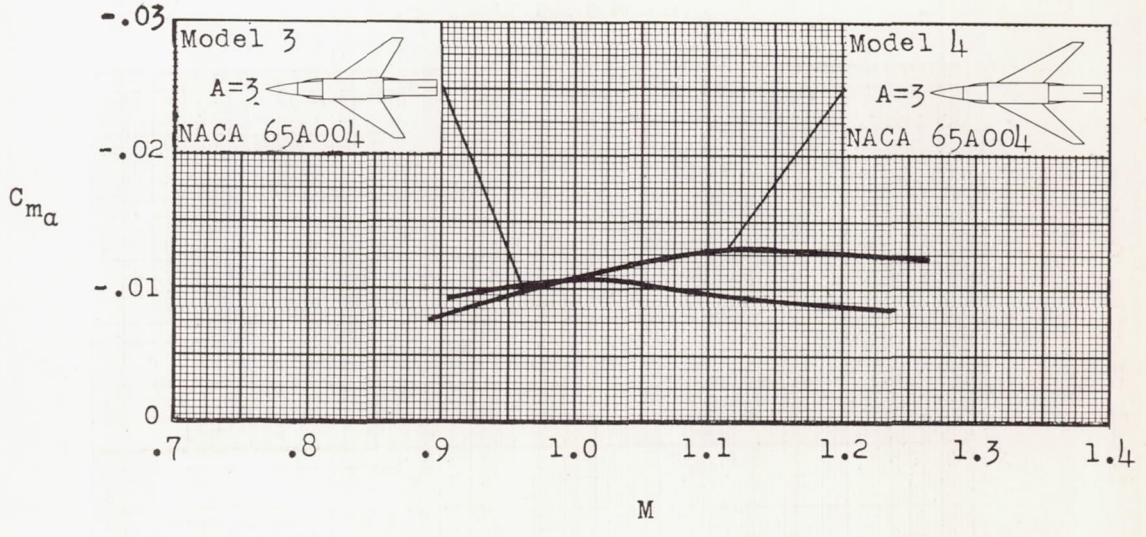

(b) Models 3 and 4.

Figure 11.- Variation of the slope of the pitching-moment curve with Mach number.

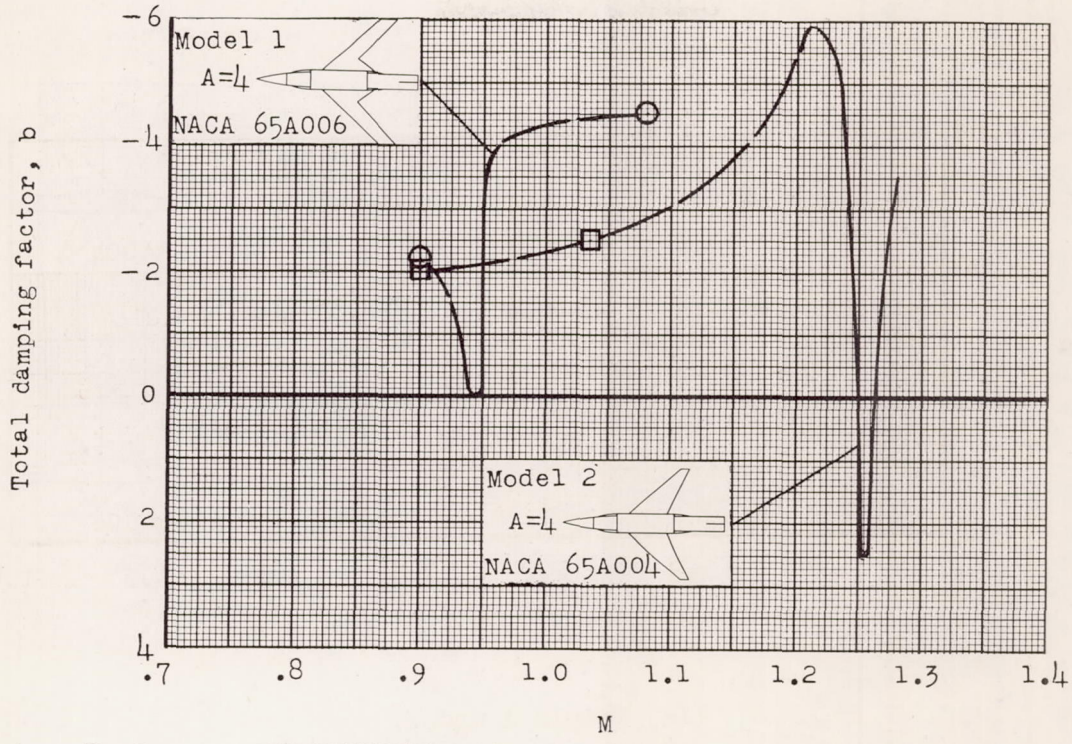

(a) Models 1 and 2.

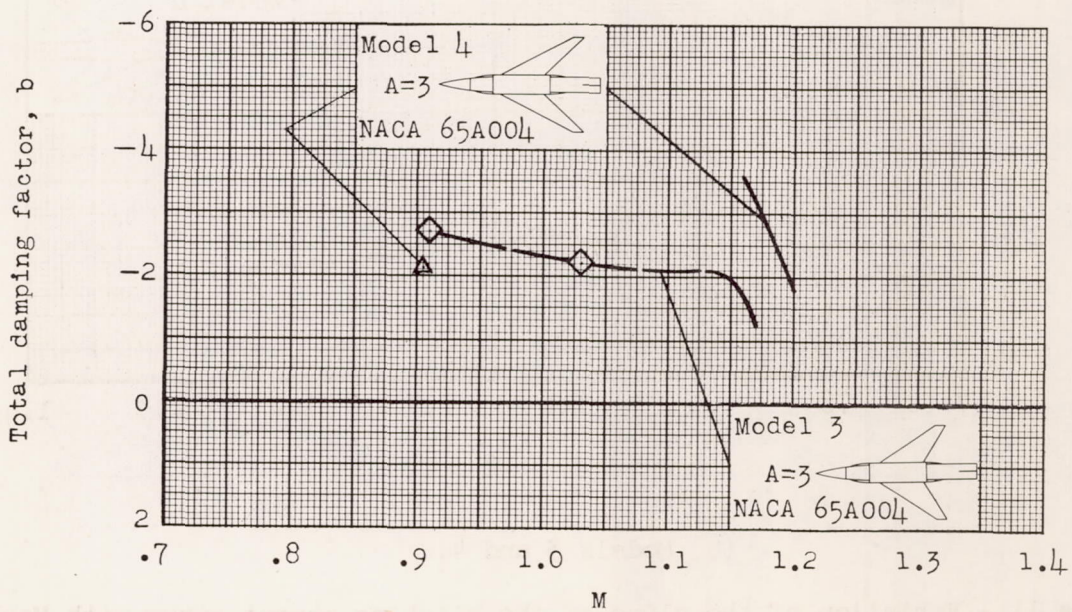

(b) Models 3 and 4.

Figure 12.- Variation of the total damping factor with Mach number.

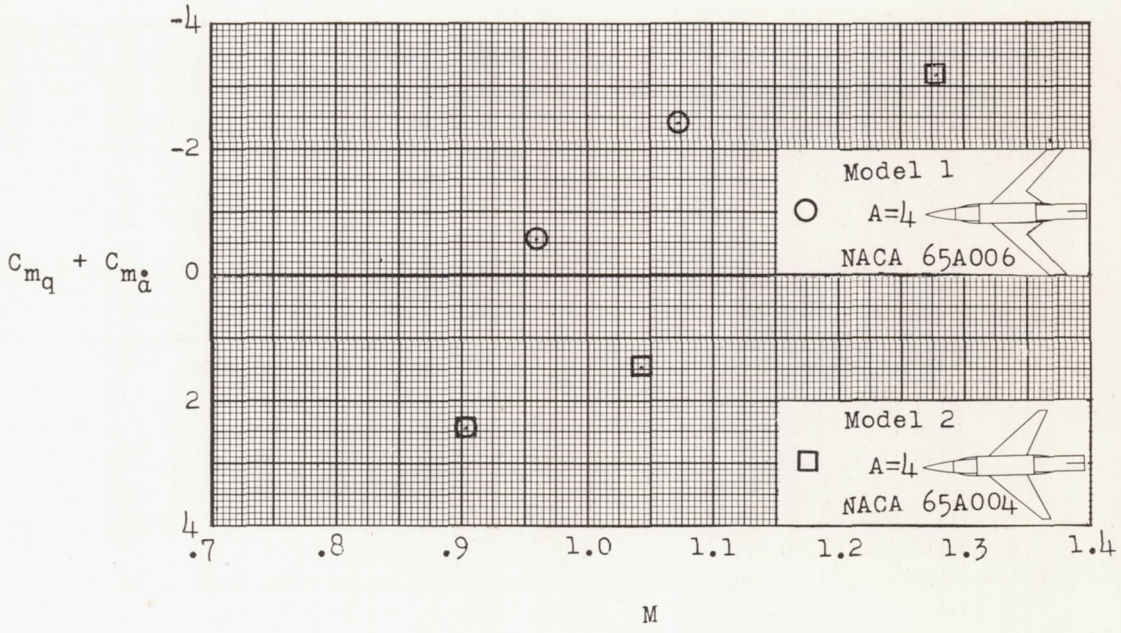

(a) Models 1 and 2.

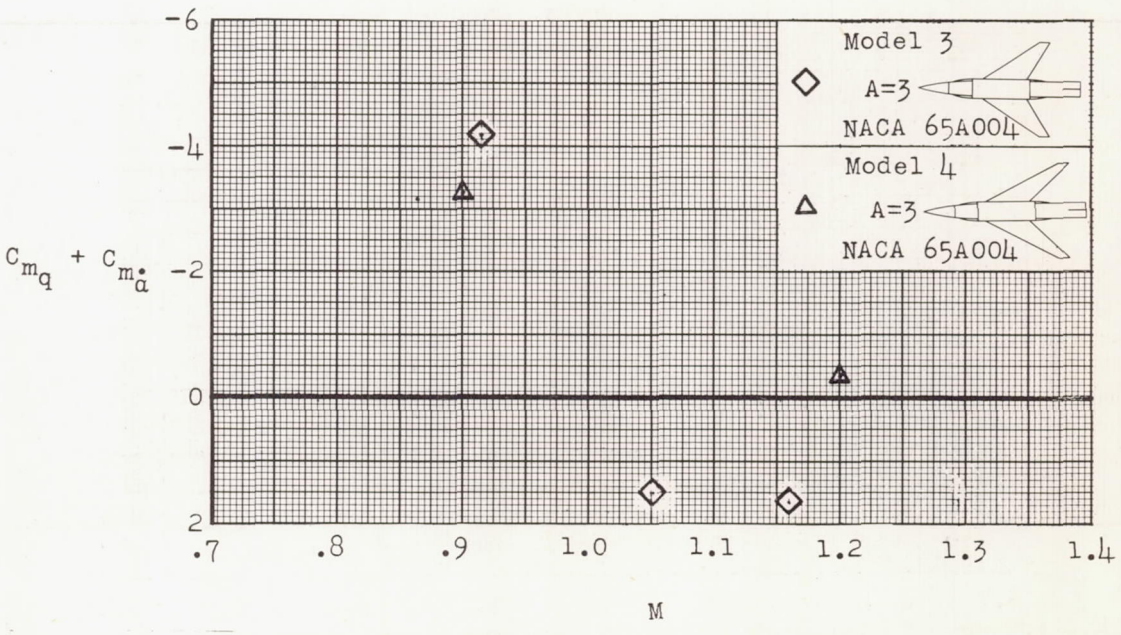

(b) Models 3 and 4.

Figure 13.- Variation of the rotational damping-in-pitch derivatives with Mach number.

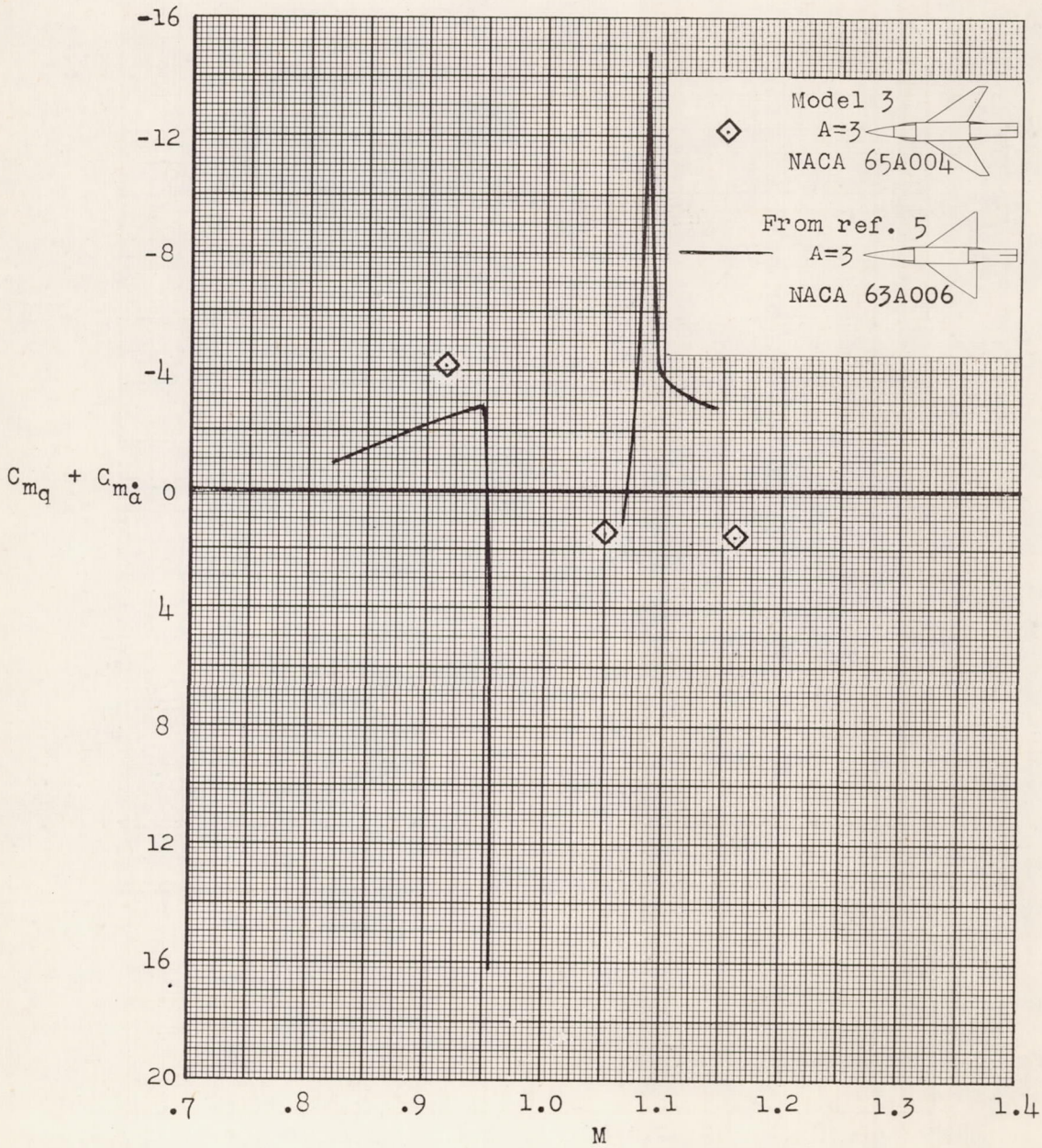

Figure 14.- Effect of plan-form shape on the rotational damping-in-pitch derivatives.

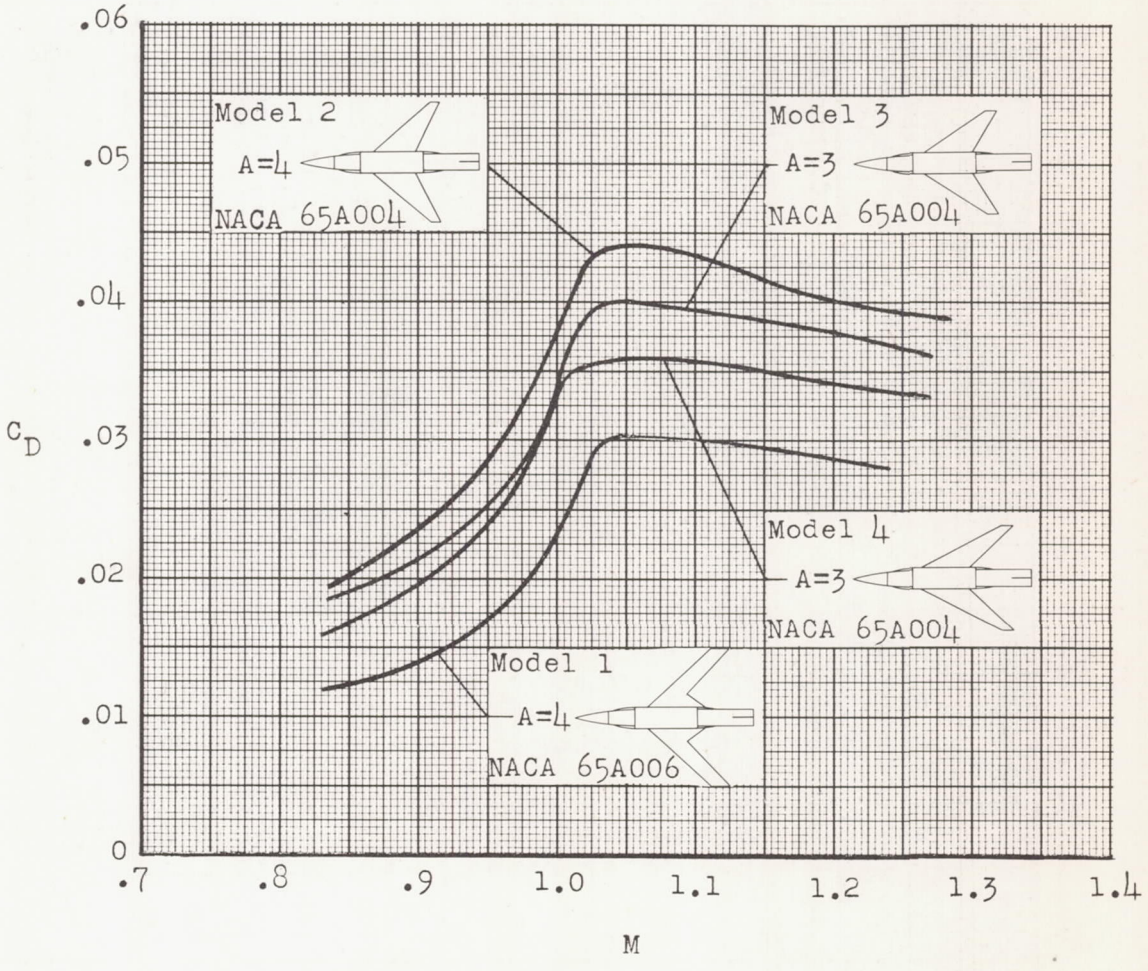

Figure 15.- Variation of the drag coefficient with Mach number.

NACA-Langley - 11-24-54 - 300